Indian Journal of Chemistry
Vol. 57A, November 2018, pp. 1335-1343

Microwave-assisted synthesis of nitrogen-doped ZnO nanoparticles: Characterization and its comparative study on sonocatalytic, photocatalytic and sonophotocatalytic degradation of amido black

Srishti Kumawat[a], Nutan Salvi[a], Kiran Meghwal[a], Rakshit Ameta[b], Chetna Ameta[a,]*

[a]Photochemistry Laboratory, Department of Chemistry, University College of Science, M. L. Sukhadia University, Udaipur 313 001, Rajasthan, India
[b]Department of Chemistry, J. R. N. Rajasthan Vidyapeeth (Deemed-to-be University), Udaipur 313 001, Rajasthan, India
Email: chetna.ameta@yahoo.com

Received 22 May 2018; revised and accepted 15 October 2018

Nano rods like N-doped ZnO structures have been prepared using microwave-assisted method. Synthesized nanoparticles have been characterized by Field Emission Scanning Electron Microscopy (FESEM), Transmission Electron Microscopy (TEM), X-ray diffraction (XRD), energy dispersive X-ray (EDX), Fourier-transform Infrared Spectroscopy (FTIR) and ultraviolet-visible (UV-vis) spectroscopy. The N-doped ZnO catalyst has been further used for the degradation of amido black-10B (a non-biodegradable azo dye) using photocatalysis and sonocatalysis systems, separately and simultaneously. The experimental kinetic data followed the pseudo-first order model in photocatalytic, sonocatalytic and sonophotocatalytic processes but the rate constant of sonophotocatalysis has been found higher than the rate constants of photocatalysis and sonocatalysis processes due to the formation of more reactive radicals as well as active surface area of the catalyst.

Keywords: Amido black-10B, Photocatalysis, Sonocatalysis, Sonophotocatalysis

Water pollution is an appalling problem and is powerful enough to push the world on the path of destruction. Wastewater contains hazardous organic pollutants such as polychlorinated biphenyls (PCBs), solvents, dyes, pesticides, etc., from various industries which cause severe environmental pollution. Due to their stability and chemical structure, the organic dyes in the effluents coming from these industries are difficult to degrade. Of nearly 8,00,000 tonnes of dyes produced in the world on a yearly basis, 50% comes from azo dyes[1].

Under anaerobic conditions, azo dyes, in particular, may partially break down to yield aromatic amines, most of which have been labelled as toxic, carcinogenic, mutagenic and genotoxic[2,3]. Nowadays, various chemical and physical processes such as elimination by adsorption onto activated carbon, coagulation by a chemical agent, ozone oxidation, hypochlorite oxidation, electrochemical method, etc., are applied in order to treat the dye waste effluents[4-6]. Nevertheless, these methods result in the production of secondary waste products and are usually non-destructive, inefficient and costly. Therefore, purification of azo dye wastewater has become a matter of great concern and it is absolutely necessary to develop novel and cost-effective technologies to treat azo dye wastewater.

Advanced oxidation processes (AOPs) have shown a great potential as a low-cost and efficient wastewater treatment technology as these have the potential to completely mineralize organic compounds to CO_2 and H_2O[7]. A strong oxidizing species $^{\bullet}OH$ radicals produced *in situ* are normally utilized by AOP triggering a sequence of reactions that break down the dye macromolecule into smaller and less harmful substances. This process is also called as mineralization[8-10]. In wastewater treatment, AOPs, usually introduce a specific subset of processes that involve O_3, H_2O_2 and/or UV light. However, AOPs also involve photocatalytic oxidation, ultrasonic cavitation, electron-beam irradiation and Fenton's reaction, which could also be used to refer to a more general group of processes. Various combinations of them are employed for the complete mineralization of pollutants.

The enhancement of photocatalytic degradation of organic dyes such as methylene blue and methyl

orange in the presence of ZnO/CuO nanocomposites was reported by Saravanan *et al.*[11] Shahrezaei *et al.*[12] studied photocatalytic degradation of aniline in the presence of titanium dioxide (TiO_2). Sin *et al.*[13] investigated the photocatalytic activity of europium-doped ZnO for degradation of phenol.

Farhadi and Siadatnasab[14] carried out the sonocatalytic degradation of three organic pollutants including methylene blue (MB), rhodamine B (RhB) and methyl orange (MO) using CdS nanoparticles. The sonochemical degradation of Basic Blue 41 dye assisted by nano-TiO_2 and H_2O_2 as a catalyst was reported by Abbasi and Asl[15]. Khataee *et al.*[16] investigated the sonocatalytic activity of synthesized TiO_2-biochar nanocomposite using reactive blue 69 dye. The sonocatalytic degradation of humic acid by N-doped TiO_2 nanoparticle in aqueous solution was investigated by Kamani *et al.*[17]

Berberidou *et al.*[18] investigated sonolytic, photocatalytic and sonophotocatalytic degradation of malachite green using TiO_2. Sonophotocatalytic degradation of trypan blue and vesuvine dyes in the presence of Ag_3PO_4/Bi_2S_3 based photocatalyst was reported by Mosleh *et al.*[19] Taufik *et al.*[20] reported comparison of the rate of degradation of methylene blue under sonocatalytic, photocatalytic and sonophotocatalytic condition. For this, they synthesized Fe_3O_4/CuO/ZnO nanocomposites as a catalyst by sol-gel method. The performance of ZnO nanoparticles decorated with multi-walled carbon nanotubes on the photocatalytic, sonocatalytic and sonophotocatalytic degradation of rhodamine B was studied by Ahmad *et al.*[21]

Among various photocatalysts, ZnO and TiO_2 utilise a small portion of solar energy (3–5%) in the UV region owing to their large band gap[22-25]. But these are very important due to their high photosensitivity, nontoxicity and low cost. Since some researchers have mentioned that zinc oxide is much more efficient than titanium dioxide, particularly for photocatalytic degradations of azo dyes[26], pulp wastewaters[27,28], and phenols[29] under UV irradiation, it is anticipated that as compared to TiO_2, nanostructured ZnO can become a versatile alternative. For desired band-gap narrowing and an enhancement in the photocatalytic efficiency, ZnO photocatalysts involve some modification like doping with non-metal elements. Of the non-metal elements, N seems to be a suitable dopant due to its similar size with O and its lower electronegativity than that of O[30].

The aim of this work was to synthesize N doped ZnO (NZO) through wet chemical method. The photocatalytic activity of NZO was evaluated for the degradation of amido black 10B (AB) by means of sonocatalysis, photocatalysis and their combined application, sonophotocatalysis, concerning the effect of key operating conditions on the kinetics of dye conversion and sample mineralization. The effects of pH, amount of photocatalyst and the concentration of amido black 10B were examined.

Materials and Methods

Zinc acetate dihydrate (ZAD) (SRL), hydrazine dihydrochloride (Thomas Baker), and NH_4OH solution were used in the present investigation. Amido Black-10B (AB) (HiMedia laboratories ltd, Mumbai, India) has been chosen as a representative model compound. AB is a non-biodegradable synthetic azo dye with a molecular formula $C_{22}H_{14}N_6Na_2O_9S_2$, widely used in textile industry. All the chemicals used were of laboratory grade. All solutions were prepared in doubly distilled water.

Synthesis of NZO nanoparticles was carried out by the wet chemical method[31,32] using a microwave. The requisite precursor solution was prepared to take the starting materials of host and dopant sources. For this, zinc acetate dihydrate ($Zn(CH_3COO)_2.2H_2O$) of zinc sources and hydrazine dihydrochloride ($N_2H_4.2HCl$) of nitrogen source were taken. 0.5 M zinc acetate dihydrate (ZAD) and 0.1 M hydrazine dihydrochloride were mixed in deionized water and magnetically stirred until complete dissolution.

The required amount of ammonia solution was added drop by drop to the prepared solution with constant stirring until a clear solution was obtained. The pH and amount of ammonia were maintained for all these solutions. The quantity of ammonia solution used was 120 mL and the final pH of the solution obtained was 8.0. The prepared solution was irradiated with a microwave synthesizer (Electrolux-EM 20 EC) for 3-4 mins at 800 W. After 3 min, the precipitate settled down at the bottom of the container and was allowed to cool down overnight in alcohol. The precipitate was collected with the help of Whatman filter paper in a Buchner funnel and was repeatedly washed with distilled water and alcohol. It was then dried in an oven for 2 to 3 h at 110 °C. For undoped ZnO (ZO), the synthesis procedure was carried out without adding hydrazine dihydrochloride.

The crystallinity of NZO powder was determined by X ray diffraction (XRD) using Rigaku Ultima IV with Cu-Kα radiation in the range $2\theta = 10–90^o$. The

accelerating voltage and the applied currents were 40 kV and 40 mA, respectively. The data obtained from the XRD measurements were matched with the standard JCPDS data (card no-00-005-0664) and all the well-defined diffraction peaks are indexed accordingly. The morphology of the synthesized nanoparticles of NZO was studied by FESEM. It was recorded on the Hitachi SU8010 FESEM. Transmission electron microscopy (TEM) study on the microstructure of NZO was carried out on a TEM-Tecnai G2 20 instrument. The nanoparticles were examined by recording their IR spectra employing a Bruker OPUS 7.5.18 FTIR spectrophotometer. UV-visible reflectance mode spectra of prepared nanoparticles were recorded in the wavelength range 200–800 nm using Perkin-Elmer Lambda-750 UV–visible spectrophotometer.

In this study, degradation of AB dye, used as a pollutant was investigated in the presence of NZO nanoparticles using 200 W tungsten lamp (photocatalysis) and ultrasonic bath (sonocatalysis) systems separately and simultaneously (sonophotocatalysis). A stock solution of AB (1.0×10^{-3} M) was prepared in doubly distilled water. The reaction suspension was prepared by adding 0.15 g of the photocatalyst in 50 mL of 2.5×10^{-5} M AB solution. This mixed solution was kept in dark for an hour to establish an adsorption-desorption equilibrium on the photocatalyst before light irradiation. The solution was then irradiated with visible light using a 200 W tungsten lamp. For the measurement of light intensity (in the unit of mW cm^{-2}), a solarimeter (Surya Mapi Model CEL 201) was used. The maximum light intensity was measured by varying the distance between the exposed surface of the reaction vessel and the filament of the lamp. The maximum rate of degradation of AB dye was found at 60.0 mW cm^{-2} for both doped and undoped ZnO. The sonocatalytic and sonophotocatalytic degradation was estimated by catalyst with a rectangular shaped ultrasonic bath (systronic model 392) filled with water operating at a fixed frequency of 40 kHz and an ultrasonic power of 200 W. All runs were carried out under atmospheric conditions and by continuously stirring the reaction mixture. A water filter was used to cut off thermal radiations. A digital pH meter (Systronics Model 335) was used to measure the pH of the reaction mixture. Sulphuric acid (0.1 N) and sodium hydroxide 0.1 N solutions which were previously standardized were added to adjust the pH of the solution. Prior to measurement of optical density, NZO particles were separated using a centrifuge. Different water quality parameters like dissolved oxygen, salinity, TDS, conductivity and pH of polluted and treated water were determined by using water analyser (Systronics Model 371). Chemical oxygen demand (COD) of AB dye solution was estimated before and after the sonophotocatalytic treatment by a standard dichromate method using COD digester. The percentage of photodegradation efficiency (η) was calculated from the following expression

$$\eta = \frac{COD_{before} - COD_{after}}{COD_{before}} \times 100 \quad \text{... (1)}$$

The absorbance of samples was observed before starting the run and at different intervals of time using UV visible spectrophotometer Model 2371 at 618 nm (λ_{max} of amido black).

Results and Discussion

X-ray diffraction (XRD) pattern shows the presence of sharp, narrow and distinct peaks which provided the direct evidence of the crystalline nature of the prepared N doped ZnO (Fig. 1). XRD data analysis showed that N doped ZnO crystallizes in the wurtzite type hexagonal structure of zinc oxide (where a = b = 3.25552 Å and c = 5.21579 Å. a, b and c are edge lengths of unit cell along three axes). The prominent diffraction peaks from crystal planes (100), (002), (101), (102), (110), (103) and (112) planes are shown in Fig. 1. The peak at 36.195° corresponds to the 101 plane and is the most intensive peak in XRD patterns which suggested that NZO nanorods grew along (101) direction. Additional peaks at 31.7°, 34.3°, 47.4°, 56.5°, 62.7° and 68.0° which could be assigned to (100), (002), (102), (110), (103) and (112) planes of wurtzite NZO respectively, were also observed, and no peaks related to any other impurity were detected for N doped ZnO.

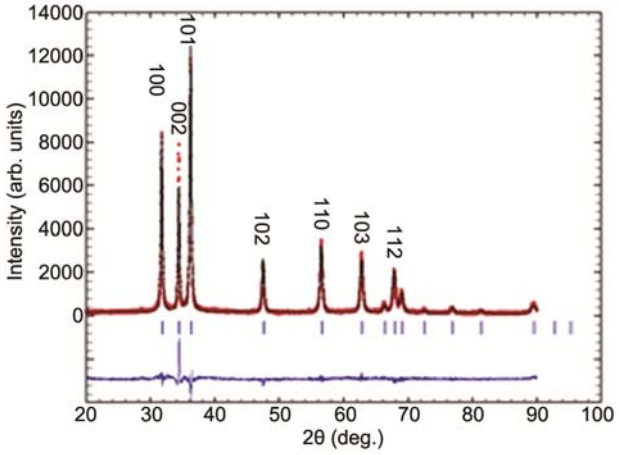

Fig. 1 — XRD pattern of N doped ZnO.

Average crystallite size for NZO was 31.99 nm whereas for undoped ZnO, it was found to be 34.67 nm. Both were calculated using Scherrer's formula ($D = k\lambda/\beta\cos\theta$ where D is the crystallite size, k is the wavelength of radiation, β is the peak full width at half maximum (FWHM), θ is the diffracting angle and k = 0.94). The FESEM micrographs of these synthesized samples are shown in Fig. 2. The NZO particles are uniform and have an overall good regularity on observed surface (Fig. 2(a)). Upon closer examination, we observe that the hexagonal N doped zinc oxide (NZO) (Fig. 2(e)) are like nanorods. These nanorods have 'pencil-like tip' at both ends (Fig. 2 (d)). Nanorods formed, are either separate or mostly occur as a cluster of agglomerated rods (Fig. 2(b)). These rods assemble to form flower-like structures (Fig. 2(c)).

EDX spectroscopy was performed to confirm the presence of N and for compositional analysis of nanoparticles. The obtained result of NZO was found to be 0.80 w% for N, 19.64 w% for O, 85.86 w% for zinc (Fig. 3). This result confirms the content of the N incorporated in ZnO.

The TEM image of the N-doped ZnO powder has been shown in Fig. 4. TEM image (Fig. 4c) and the corresponding Selected-Area Electron Diffraction (SAED) pattern in Fig. 4a and 4b reveal that the nanorods are single crystalline and no amorphous products are found on the surface of the nanorods. The size of the primary particles, estimated from the TEM image was about 20–50 nm and was in good agreement with the value (31.99 nm) which was calculated from XRD pattern using the Scherrer equation. FTIR spectrum of the NZO shows intense, broad peak near 3360 cm^{-1} representing the hydrogen bonded O-H stretching vibration[33] (Supplementary Data, Fig. S1). Two peaks at 1390 and 1502 cm^{-1} for NZO sample may be assigned to the vibration of the Zn-N bonds[34], indicating that the doping of ZnO with nitrogen was successful. This spectrum also shows absorption peaks

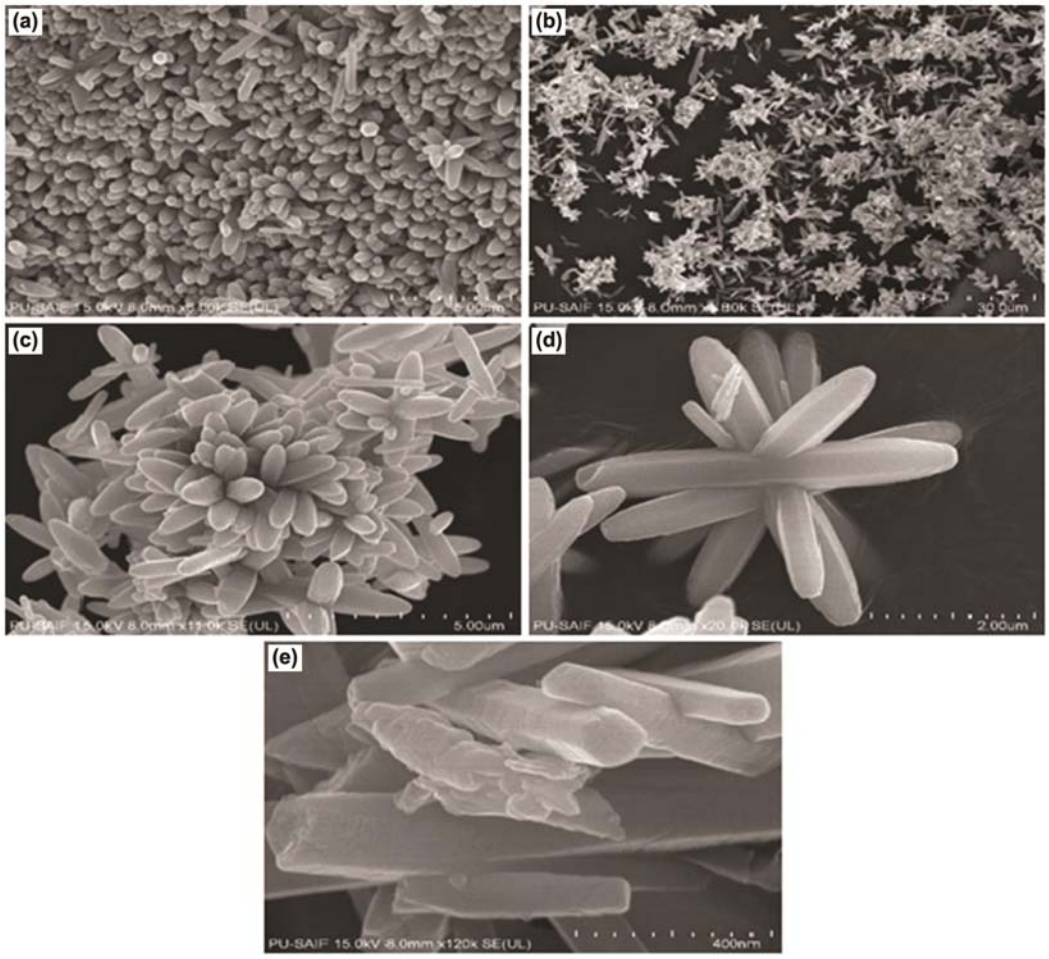

Fig. 2 — FESEM of N doped ZnO at a distance of (a) 5.00 µm (b) 30.0 µm (c) 5.00 µm (d) 2.00 µm, and, (e) 400 nm.

below 600 cm^{-1}, which correspond to the characteristic absorption of Zn-O bond in zinc oxide[35,36].

In UV-DRS (Ultraviolet-diffuse reflectance spectroscopy), the band gap energy (in eV) of nanoparticles was estimated by employing Kubelka-Munk (K-M) function[37] (Supplementary Data, Fig. S2).

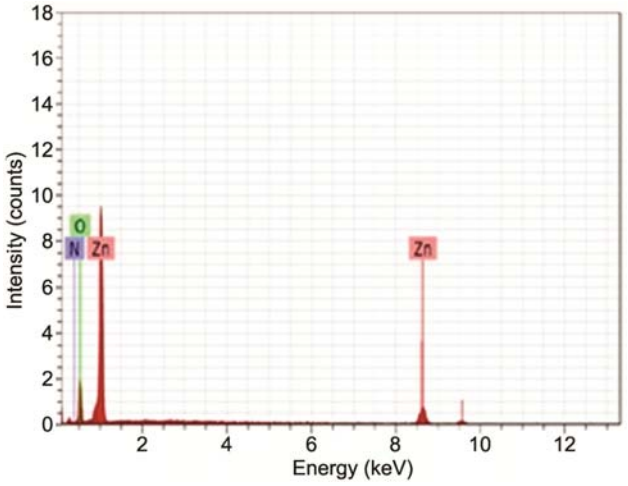

Fig. 3 — EDX spectra of N doped ZnO.

The band gap of powder sample can be extracted by plotting $(K/S\ (hv))^2$ against energy (eV) (Supplementary Data, Fig. S3). S and K are respectively called as 'K-M scattering' and 'absorption' coefficients[38,39] hv is the photon energy[39]. Band gap energy of undoped and N-doped ZnO is found to be 3.30 and 3.13 eV, respectively. Here, N-doped ZnO absorbs longer wavelength (visible) light as compared to undoped ZnO as its band gap is less. The contribution of nitrogen to the top of the valence band (VB) of ZnO plays the major role of extending the absorption of N-doped ZnO to the visible region.

The effect of pH on the rate of sonocatalytic, photocatalytic and sonophotocatalytic degradation of AB was investigated in the range 7.0–10.5 (Supplementary Data, Table S1). The pH of the suspension was adjusted before irradiation and it was not controlled during the irradiation. The results are reported in Fig. 5(a). In all three cases, the synergy in degradation is significantly higher in the alkaline range compared to that at lower pH and it attained

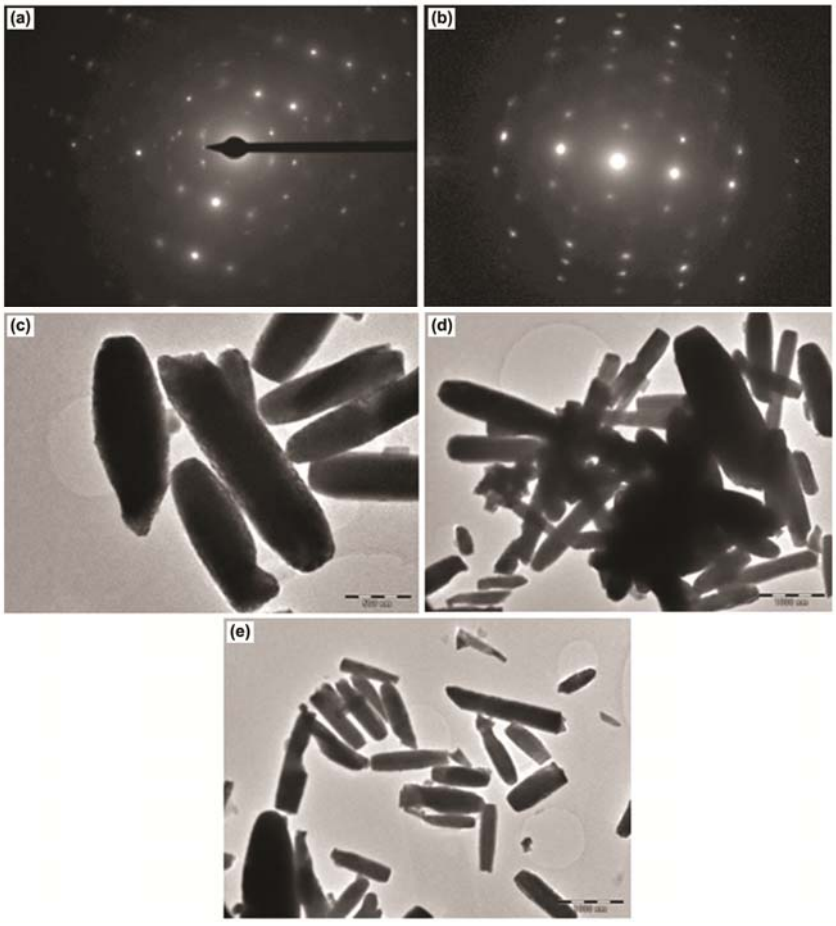

Fig. 4 — TEM images of N doped ZnO where (a) and (b) show SAED pattern; (c) captured at 500 nm and (d), (e) captured at 1000 nm.

Table 1 — Kinetic analysis (Typical run)

Time (min)	In the presence of NZO			In the presence of ZO
	AB+US[a]+NZO	AB+VL[b]+NZO	AB+US+VL+NZO	AB+US+VL+ZO
	2+ log*A*	2+ log*A*	2+ log*A*	2+ log*A*
0	1.759	1.759	1.759	1.759
10	1.710	1.698	1.568	1.671
20	1.637	1.607	1.421	1.655
30	1.614	1.534	1.324	1.603
40	1.605	1.498	1.130	1.534
50	1.578	1.436	0.96	1.449
60	1.565	1.356	0.745	1.447
70	1.512	1.278	0.54	1.386
80	1.507	1.198	0.378	1.351
90	1.460	1.167	0.19	1.291
100	1.439	1.127	0.0146	1.201
k value	1.11×10^{-4} (s^{-1})	2.56×10^{-4} (s^{-1})	6.70×10^{-4} (s^{-1})	1.99×10^{-4} (s^{-1})

[AB] = 2.5×10^{-5} M, pH = 9.0, NZO = 0.15 g, ZO = 0.15 g

[a]ultrasonic irradiation, [b]visible light

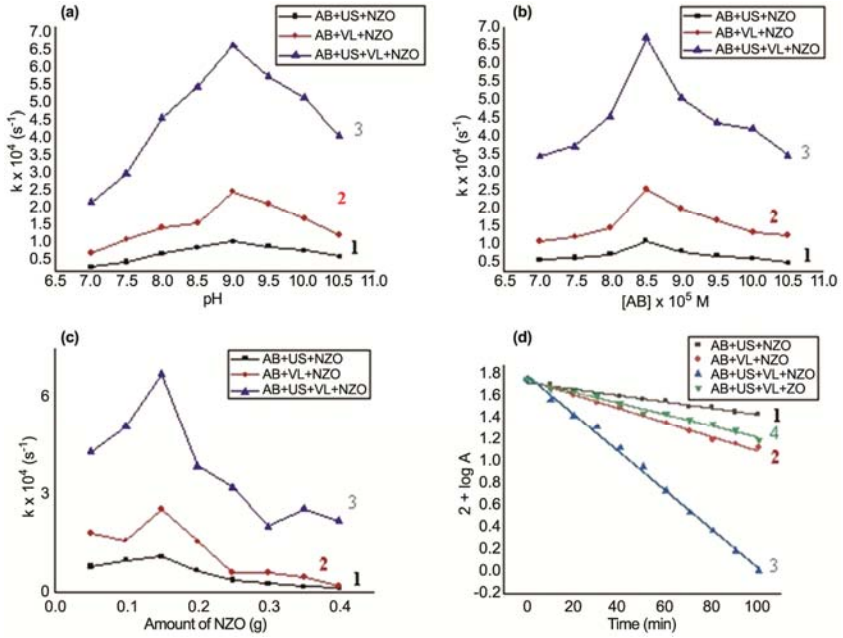

Fig. 5 — (a) Effect of pH variation (plotted between pH and $k\times10^4$ (s^{-1}) at optimum condition for [Amido black 10 B] = 2.5 M and catalyst= 0.15 g) (b) Effect of dye concentration (plotted between [Amido black 10 B]$\times10^5$ M and $k\times10^4$ (s^{-1}) at optimum condition for pH = 9 and catalyst = 0.15 g), (c) Effect of catalyst loading (plotted between catalyst amount and $k\times10^4$ (s^{-1}) at optimum condition for pH = 9 and [Amido black 10 B] = 2.5 M), (d) Typical run, and curve 1 for sonocatalytic degradation of AB in presence of NZO, curve 2 for photocatalytic degradation of AB in presence of NZO, curve 3 for sonophotocatalytic degradation of AB in presence of NZO, curve 4 for sonophotocatalytic degradation of AB in presence of ZO.

optimum value at pH 9. The rate decreased when pH of the dye solution was further increased. It may be because of the fact that the cationic dye molecules and negatively charged $^{-}$OH ions attract each other on increasing the pH of the solution. But, at higher pH, the cationic dye molecules convert into neutral form and hence, there is less attraction between neutral dye molecule and the negatively charged surface of the semiconductor. As a result, the rate was retarded. The rate of sonophotocatalytic degradation was comparatively higher than sonocatalysis and photocatalysis alone due to combined effects of sonocatalysis and photocatalysis, there is a greater probability for the formation of hydroxyl radicals ($^{\bullet}$OH radicals) and these $^{\bullet}$OH radicals are actual oxidizing species responsible for the degradation of dye.

The concentration of dye for optimum degradation of AB has been experimentally determined for sono,

photo and sonophotocatalysis, respectively (Fig. 5(b) and Supplementary Data, Table S2). At a different concentration of dye, keeping all other factors identical, it had been observed that the value of rate constant increases with increase in the concentration of solution and reaches an optimum range i.e., 2.5×10^{-5} M. Beyond this optimum, the degradation slows down and thereafter remains more or less steady or even decreases in all three cases. This may be explained on the basis that, on increasing the concentration, the availability of dye molecules increases with respect to $^{\bullet}$OH radicals and hence the rate of reaction increases. But after optimum concentration, reaction rate decreased because the number of collisions between dye molecules increase and collisions between the dye and $^{\bullet}$OH radicals decrease. The efficiency of degradation of dye was found in the order: sonophotocatalysis > photocatalysis > sonocatalysis. The enhancement in the AB degradation by the combined effect of photocatalysis and sonolysis i.e., sonophotocatalysis produced a synergistic effect, which is further explained by the increase in mass transport of chemical species between the solution phase and the catalyst surface and the additional yields of $^{\bullet}$OH radicals by acoustic cavitation[40,41].

In order to determine the effect of catalyst loading on dye degradation efficiency, experiments were performed with different catalyst amounts using an initial concentration of 2.5×10^{-5} M of AB dye at pH 9 (Supplementary Data, Table S3). The amount of catalyst is an important parameter that can affect the degradation rate of organic compounds. The catalyst concentration of NZO ranges from 0.05 to 0.4 g. It was observed that initially, the degradation rate increases up to optimum concentration of 0.15 g of NZO catalyst as shown in Fig. 5(c). The enhanced degradation efficiency is probably due to an increased number of adsorption sites and more effective interaction with the irradiation which leads to higher number of reactive hydroxyl radicals. Thereafter, rate decreases on increasing the amount of catalyst. This may be due to the aggregation of catalyst particles causing a decrease in the number of available active surface sites. The particles do not suspend fully and effectively beyond a particular loading in a particular reactor which also leads to suboptimal penetration of irradiation and reduced adsorption of the substrate on the surface. However, the optimum loading is slightly higher at 0.15 g in sonophotocatalysis compared to sonocatalysis and photocatalysis.

Table 2 — Quality parameters of water

Various parameters	Before sonophotocatalytic treatment	After sonophotocatalytic treatment
DO (ppm)	0.1	4.5
Conductance (μS)	23.5	352
Salinity (ppt)	0.02	0.39
TDS (ppm)	12.3	233
pH	4.5	7.2
COD (ppm)	413	93.6

After keeping the values of the above parameters constant for the maximum rate constant, a typical run was observed by plotting a graph between $2 + \log A$ and time (in minutes) where A is absorbance of the dye solution. Like photocatalysis, sonocatalysis and sonophotocatalysis also appear to follow a pseudo-first order kinetics. The rate constant (k) was measured using the expression

$$k = 2.303\times\text{slope} \quad \text{... (2)}$$

The results are shown in Table 1. Here, a comparative observation was made for photocatalysis, sonocatalysis and sonophotocatalysis by using N doped ZnO, which confirms that the rate of sonophotocatalysis was highest and sonocatalysis was lowest. $k_{sonophoto}$ was almost six times higher than k_{sono}, and k_{photo} is approximately 2.5 times higher than k_{sono}. The rate constants for NZO is in the following order: $k_{sonophoto} > k_{photo} > k_{sono}$.

Additionally, a typical run was also conducted for sonophotocatalysis using undoped ZnO (ZO) under (Table 1 and Fig. 5(d)) and the rate of sonophotocatalysis for NZO was still greater than undoped ZnO under optimum condition of pH, dye concentration and catalyst loading.

Various quality parameters were measured for sample solution of AB dye before and after sonophotocatalytic treatment[42,43]. Quality parameters were taken only for sonophotocatalysis because the best results for the rate of degradation of dye were obtained in sonophotocatalysis only. The values of dissolved oxygen (DO), conductance, salinity, total dissolved solids (TDS), pH and chemical oxygen demand (COD) are given in Table 2. Dissolved oxygen analysis measures the amount of gaseous oxygen (O_2) dissolved in water. The amount of dissolved oxygen was 0.1 ppm before degradation and after sonophotocatalytic treatment, the amount of dissolved oxygen increased to 4.5 ppm, which indicates mineralization of dye to a significant extent.

The more the ions, the greater the conductivity and hence, conductivity can be used as a measure of the level of ion concentration of a solution. Conductivity increased after the sonophotocatalytic treatment, which indicates that the dye has been mineralized into smaller molecules/ions like CO_2, NO_3^-, SO_4^{2-} etc. Because of the same reason, total dissolved solids and salinity of the dye solution was also found to increase. pH of reaction mixture was acidic before treatment but after sonophotocatalytic degradation of the dye, pH becomes almost neutral, clearly showing that the dye particles are mineralized to a significant extent. The COD value of 413 ppm for 2.5×10^{-5} M dye concentration decreased to 93.6 ppm (77.3% dye degradation) after 1 h of irradiation.

On the basis of the experimental observation, the following tentative mechanism has been proposed for sonophotocatalytic degradation of Amido black 10B (AB). AB dye molecule absorbs radiation of suitable wavelengths and it is excited to its first singlet excited state followed by intersystem crossing (ISC) to the triplet state.

$$AB_0^1 + h\nu \rightarrow AB_1^1 \text{ (singlet excited state)} \quad \ldots (3)$$

$$AB_1^1 \xrightarrow{ISC} AB_1^3 \text{ (triplet excited state)} \quad \ldots (4)$$

The semiconductor (SC) will be excited on exposure of visible light and/or ultrasound to give SC*. This excited state will provide an electron (e^-) in the conduction band and a hole in the valence band. This hole may abstract an electron from hydroxyl ions to generate hydroxyl radicals. The dye molecules will then be oxidized by these hydroxyl radicals to harmless products. The degradation rate of amido black will enhance due to the generation of more $^\bullet$OH radicals in presence of ultrasound by sonolysis of water. The $^\bullet$OH radicals participate as an active oxidizing species and it was confirmed by carrying out the same reaction in presence of some hydroxyl radical scavengers like isopropanol, where the rate of degradation was drastically reduced.

$$SC + h\nu \rightarrow e^- (CB) + h^+ (VB) \quad \ldots (5)$$

$$h^+ + {}^-OH \rightarrow HO^\bullet \quad \ldots (6)$$

$$HO^\bullet + AB_1^3 \rightarrow \text{smaller products} \quad \ldots (7)$$

Conclusions

Nitrogen-doped ZnO nanoparticles prepared via a simple microwave assisted method proved to be efficient in removal of amido black dye. The catalyst exhibited good photocatalytic, sonocatalytic and sonophotocatalytic activity. Although photocatalytic degradation alone is considerably faster (by about an order of magnitude) than sonocatalytic degradation, efficiency can be further improved by coupling the two processes. The beneficial synergy of process integration is a conceptually advantageous approach in AOP-based water treatment, which can be attributed to the formation of more reactive radicals as well as the increase of the active surface area. The optimum pH and catalyst amount for the efficient removal of dye are found to be 9.0 and 2.5 g L^{-1}, respectively. The kinetics of the degradation in all three cases in the presence of the nanocatalysts followed first-order rate model. COD reduction of dye confirms the destruction of the organic molecules.

For comparative study, sonophotocatalysis activity was also carried out under optimum conditions using undoped ZnO. Here, it was observed that the rate of degradation was lower than the rate achieved using NZO. Therefore, the NZO nanoparticles are exceptional materials for applications in a number of environmental issues such as treatment of wastewater.

Acknowledgement

The authors are thankful to DST FIST schemes of the Department of Physics, M.L. Sukhadia University, Udaipur, India for providing XRD characterisation. We are also thankful to UGC-DAE Consortium, Indore for providing TEM facility and SAIF Chandigarh for providing FESEM, EDX, UV-DRS facilities. Authors thank the Head, Department of Chemistry, M. L. Sukhadia University, Udaipur, India for providing laboratory facilities.

Supplementary Data

Supplementary data associated with this article, are available in the electronic form at http://www.niscair.res.in /jinfo/ijca/IJCA_57A(XX)1335-1343_SupplData.pdf.

References

1 Zollinger H, *Color chemistry: syntheses, properties and applications of organic dyes and pigments*, (VCH Publishers, New York) 1991.
2 Meric S, Selcuk H, Gallo M & Belgiorno V, *Desalination*, 173 (2005) 239.
3 Vilar V J P, Pinho L X, Pintor A M A & Boaventura R A R, *Sol Energ*, 85 (2011) 1927.
4 Tanaka K, Padermpole K & Hisanga T, *Water Res*, 34 (2000) 327.
5 Yoshida Y, Ogata S, Nakamatsu S, Shimamune T, Kikawa K, Inoue H & Iwakura C, *Electrochim Acta*, 45 (1999) 409.

6 Shen Z, Wang W, Jia J, Ye J, Feng X & Peng A, *J Hazard Mater*, 84 (2001) 107.

7 Chan S H S, Wu T Y, Juan J C & Teh C Y, *J Chem Technol Biotechnol*, 86 (2011) 1130.

8 Rao A N, Sivasankar B & Sadasivam V, *J Mol Catal A: Chem*, 306 (2009) 77.

9 Rauf M A & Ashraf S S, *J Hazard Mater*, 166 (2009) 6.

10 Akyol A & Bayramoglu M, *Chem Eng Process*, 47 (2008) 2150.

11 Saravanan R, Karthikeyan S, Gupta V K, Sekaran G, Narayanan V & Stephen A, *Mater Sci Eng*, 33 (2013) 91.

12 Shahrezaei F, Mansouri Y, Zinatizadeh A A L & Akhbari A, *Int J Photoenergy*, 2012 (2012) 8.

13 Sin J C, Lam S M, Satoshi I, Lee K T & Mohamed A R, *Appl Catal B*, 148 (2014) 258.

14 Farhadi S & Siadatnasab F, *Desalin Water Treat*, 66 (2017) 299.

15 Abbasi M & Asl N R, *J Hazard Mater*, 153 (2008) 942.

16 Khataee A, Kayan B, Gholami P, Kalderis D & Akay S, *Ultrason Sonochem*, 39 (2017) 120.

17 Kamani H, Nasseri S, Khoobi M, Nodehi R N & Mahvi A H, *J Environ Health Sci*, 14 (2016) 3.

18 Berberidou C, Poulios I, Xekoukoulotakis N P & Mantzavinos D, *Appl Catal B*, 74 (2007) 63.

19 Mosleh S, Rahimi M R, Ghaedi M & Dashtian K, *Ultrason Sonochem*, 32 (2016) 387.

20 Taufik A, Tju H & Saleh R, *J Phys Conf Ser*, 2016, 710 012004.

21 Ahmad M, Ahmed E, Hong Z L, Ahmed W, Elhissi A & Khalid N R, *Ultrason Sonochem*, 21 (2014) 761.

22 Pelaez M, Nolan N T, Pillai S C, Seery M K, Falaras P, Kontos A G, Dunlop P S M, Hamilton J W J, Byrne J A, O'Shea K, Entezari M H & Dionysiou D D, *Appl Catal B*, 125 (2012) 331.

23 Chong M N, Jin B, Chow C W K & Saint C, *Water Res*, 44 (2010) 2997.

24 Liu S, Li C, Yu J & Xiang Q, *CrystEngComm*, 13 (2011) 2533.

25 Cho S, Jang J W, Lee J S & Lee K H, *Cryst Eng Comm*, 12 (2010) 3929.

26 Akyol A, Yatmaz H C & Bayramoglu M, *Appl Catal B*, 54 (2004) 19.

27 Daneshvar N, Salari D & Khataee A R, *J Photochem Photobiol A*, 162 (2004) 317.

28 Yeber M C, Rodriguez J, Freer J, Baeza J, Duran N & Mansilla H D, *Chemosphere*, 39 (1999) 1679.

29 Khodja A A, Sehili T, Ihichowski P J F & Boule P, *J Photochem Photobiol A*, 141 (2001) 231.

30 Liu G, Wang L, Yang H G, Cheng H M & Lu G Q M, *J Mater Chem*, 20 (2010) 831.

31 Kaviyarasu K, Magdalane C M, Anand, Manikandan E & Maaza M, *Spectrochim Acta, Part A*, 142 (2015) 405.

32 Yang Z Z, Liu L, Wang A J, Yuan J, Feng J J & Xu Q Q, *Int J Hydrogen Energy*, 42 (2017) 2034.

33 Seguel G V, Rivas B L & Novas C, *J Chil Chem Soc*, 50 (2005) 401.

34 Lu J, Zhang Q, Wang J, Saito F & Uchida M, *Powder Technol*, 162 (2006) 33.

35 Goswami N & Sharma D K, *Physica E*, 42 (2010) 1675.

36 Sahai A & Goswami N, *Physica E*, 58 (2014) 130.

37 Sahai A, Kumar Y, Agarwal V, Olive-Méndez S & Goswami N, *J Appl Phys*, 116 (2014) 164315.

38 Kubelka P & Munk F, *Zeitschrift für Technische Physik*, 12 (1931) 593.

39 Pankove J I, *Optical processes in semiconductors*, (Courier Corporation) 2012.

40 Suslick K S, *The chemical effects of ultrasound* (Scientific American), 260 (1989) 80.

41 Chen Y C, Vorontsov A V & Smirniotis P G, *Photochem Photobiol Sci*, 2 (2003) 69.

42 Saran S, Kamalraj G, Arunkumar P & Devipriya S P, *Environ Sci Pollut Res*, 23 (2016) 17730.

43 Iqbal M, Bhatti I A, Zia-ur-Rehman M, Bhatti H N & Shahid M, *Asian J Chem*, 26 (2014) 4291.